# Comparative Proteomic Analysis of Nicotiana Benthamiana Seedings Under Chinese Wheat Mosaic Virus Infection

**Long He**
Nanjing Agricultural University
**Peng Jin**
Ningbo University
**Xuan Chen**
Ningbo University
**Tian-Ye Zhang**
Ningbo University
**Kai-Li Zhong**
Ningbo University
**Peng Liu**
Ningbo University
**Jian-Ping Chen**
Nanjing Agricultural University
**Jian Yang** ( nather2008@163.com )
Institute of plant virology Ningbo University

**Research article**

**Keywords:** Chinese wheat mosaic virus, differentially expressed proteins, ABA, Nicotiana benthamiana

**Posted Date:** August 17th, 2020

**DOI:** https://doi.org/10.21203/rs.3.rs-47574/v1

# Comparative proteomic analysis of *Nicotiana benthamiana* seedings under *Chinese wheat mosaic virus* infection

Long He[1,2], Peng Jin[2], Xuan Chen[2], Tian-Ye Zhang[2], Kai-Li Zhong[2], Peng Liu[2], Jian-Ping Chen[1,2*], Jian Yang[2*]

[1]College of Plant Protection, Nanjing Agricultural University, Nanjing, 210095, China;

[2] State Key Laboratory for Quality and Safety of Agro-products, Institute of Plant Virology, Ningbo University, Ningbo 315211, China;

*Correspondence: Jian-Ping Chen, E-mail: jpchen2001@126.com； Jian-Yang, E-mail: nather2008@163.com

## Abstract

**Background:** *Chinese wheat mosaic virus* (CWMV) is a severe threat to winter wheat, and it is transmitted by *Polymyxa graminis*. However, the mechanisms of interactions between CWMV and plants are poorly understood. In this study, a comparative proteomics analysis based on nanoliquid chromatography (LC)- mass spectrometry (MS)/MS technique was conducted to characterize the proteomic changes of plants in response to CWMV infection.

**Results:** A total of 2,751 host proteins were identified, 1,496 of which were quantified. 146 up-regulated and 248 down-regulated proteins were identified as differentially expressed proteins (DEPs). KEGG enrichment analysis showed that the DEPs were most strongly associated with Photosynthesis - antenna proteins, MAPK signaling – plant and Glyoxylate and dicarboxylate metabolism pathways. Subcellular localization analysis showed that more than half of DEPs were predicted to be localized in the

chloroplast, an organelle indispensable for abscisic acid (ABA) synthesis. Our results suggested that CWMV infection interrupts normal chloroplast functions and decreased the contents of ABA in *Nicotiana benthamiana*. Further analysis showed that the ABA pathway was suppressed under CWMV infection and ABA treatment did induce plant hosts defense against CWMV.

**Conclusions:** In summary, our results identified several candidate proteins under CWMV infection, and the ABA pathway was deeply involved in the responses to CWMV infection in *N. benthamiana*.

**Keywords:** *Chinese wheat mosaic virus*, differentially expressed proteins, ABA, *Nicotiana benthamiana*

## Background

Plant viral infection causes severe losses in cultivated crops yield and quality during past several decades [1, 2]. Plant host resources and factors are indispensable for viral infection as plant viruses have small genomes and encode relatively few proteins [3, 4]. As a matter of fact, more and more research reveal that a variety of host factors participate in multiple steps of virus infection. For instance, *rice dwarf virus* (RDV) infection subverts auxin signaling in rice as the interaction between RDV P2 protein and OsIAA10 disrupts the interaction of OsIAA10 and OsTIR1[5]. *Rice black streak dwarf virus* (RBSDV) encoded P5-1 protein physically interacts with OsCSN5A, which interferes with the ubiquitination activity of SCF E3 ligase and suppress jasmonate signaling to benefit viral infection in rice [6].

Wheat (*Triticum aestivum* L.) is one of the most important food crops for humans worldwide [7, 8]. However, the wheat quality and yield are limited by many unfavorable factors including biotic or abiotic stresses [9]. A number of soil-borne viruses can infect wheat under natural conditions, affecting wheat growth and development [10-12]. *Chinese wheat mosaic virus* (CWMV) is a soil-borne virus first described in China [13]. CWMV is identified as a member of the genus *Furovirus* of the family *Virgaviridae*, and its genome comprises two positive sense single-stranded RNAs (+ssRNA), namely RNA1 and RNA2 [14-17]. CWMV RNA1 consists of 7,147 nucleotides (nt) and has three major predicted open reading frames (ORFs), which encodes three proteins necessary for viral replication and movement. CWMV RNA2 is 3,564 nt long and encodes four proteins: the major coat protein (CP,19 kDa), two CP-related proteins (N-CP,23 kDa and CP-RT,84 kDa) and a cysteine-rich protein (CRP,19kDa), which functions as an RNA silencing suppressor [18-20]. Besides, only a few studies have focused on the relationship between CWMV with its host during the past. Silencing *NbRDR6* reduces CWMV accumulation and siRNAs at higher temperatures [21]. NbHSP70 interacts with CWMV RNA1 encoded viral replicase and its subcellular localization was changed due to CWMV replicase [22]. CWMV derived vsiRNA-20 interferes the contents of $H^+$ in viral infected cells, resulting in CWMV accumulation [23]. It is very necessary to find potential host factors participating in the plant interaction with CWMV infection.

Quantitative proteomics approaches have been popularly developed in plant-microbe interaction study. For example, through quantitative whole-proteome analysis, Fu et al

find the expression of a remorin protein (NbREM1) is suppressed under RSV infection, and further research reveals that RSV encoded NSvc4 protein interacts with NbREM1, and it inhibits NbREM1 S-acylation to facilitate RSV infection [24]. Proteomic analysis is performed to address the effects of RBSDV on maize protein abundance, which reveals that RBSDV infection on maize is regulated by numbers of metabolic pathways [25]. Maize cv. B73 plants infected with maize chlorotic mottle virus (MCMV) has been investigated by comparative proteomic approach to get a detailed whole-proteome information that the expression levels of ribosomal proteins, proteins related to stress responses, oxidation-reduction and redox homeostasis are changed significantly under MCMV infection [26]. *N. benthamiana* is the most widely used experimental model in molecular plant-microbe interactions for it is very susceptible to multiple pathogens and amenable to transient protein expression manners and virus-induced gene silencing. It has been reported that heat shock protein 70 (HSP70) in both rice (the natural host) and *N. benthamiana* (the experimental host) are indispensable for RSV infection [27, 28]. γ b encoded by *barely stripe mosaic virus* (BSMV) is a multifunctional protein, and it can inhibit autophagy by interfering the interaction between AUTOPHAGY PROTEIN7 (ATG7) and ATG8 in *N. benthamiana* (the experimental host) [29]. Besides, artificial full-length CWMV cDNA clones have been developed which can successfully infect *N. benthamiana*, which provides a great deal of convenience for our following research [30, 31]. Although a little progress has been made in the elaborate interaction between CWMV and its plant host, there is no study on the response of plant hosts to CWMV infection at the proteomic level until now.

In the present study, we performed comparative proteomic analysis of *N. benthamiana* under CWMV infection. A certain number of DEPs were identified. We also found CWMV infection suppressed the ABA signaling pathway while ABA application induced *N. benthamiana* resistance against CWMV. Combined with virus-induced gene silencing (VIGS) technology, we found that silencing *zeaxanthin epoxidase* (*NbABA1*) or *xanthoxin dehydrogenase* (*NbABA2*) could increase CWMV accumulation probably by interfering the ABA pathway. Our study will provide candidate factors for cultivation of resistant wheat varieties and provide new insights to the molecular basis of CWMV pathogenicity.

# Results

## Overview of quantitative proteomic analysis

14 days post CWMV inoculation to four-leaf stage plants, quite a few chlorotic lesions appeared on the upper leaves of these inoculated plants (Additional file1: Fig. S1a). In addition, CWMV infection was confirmed by reverse transcription-polymerase chain reaction (RT-PCR) and western blot (Additional file1: Fig. S1b and c). These symptomatic leaves were then collected for quantitative proteomic analysis. This analysis was performed to investigate the proteomic changes of CWMV-infected compared to mock plants, and its workflow is shown as Fig. 1a. Pearson correlation coefficients indicated that biological repeat correlations were good enough (Fig. 1b). A total of 12,845 peptides were detected, and the average mass error was <0.02 Da, indicating a high mass accuracy of MS data (Fig. 1c). Moreover, the lengths of most identified peptides were distributed from 7 to 20 amino acid residues, which was

consistent with the rules based on trypsin enzymatic hydrolysis and HCD fragmentation (Fig. 1d), and thus met the quality control standard. Detailed information of identified peptides is listed in Additional file2: Table S1. In total, 2,751 proteins were identified, 1,496 of which were quantified. In order to further study the function of identified proteins, these proteins were annotated respectively according to GO terms, subcellular localizations, KEGG pathways and predicted functional domains. Detailed information of identified proteins is listed in Additional file3: Table S2.

## Impacts of CWMV infection on the *N. benthamiana* proteome

These proteins of which *p*-values$\leqslant$0.05 and mean fold-change$\geqslant$1.5 or $\leqslant$0.66 were considered as significantly differently expressed proteins (DEPs).A total of 394 proteins were identified as DEPs from those 1,496 quantified proteins. The detailed information of DEPs is listed in Additional file4: Table S3. According to the results of gene ontology (GO) analysis, 2,751 identified proteins and 394 DEPs were categorized into three major groups: biological process, cellular components and molecular function (Fig. 2a). In the biological process group, 1,290 identified proteins and 221 DEPs were involved in metabolic process, and 972 identified proteins and 168 DEPs were involved in cellular process. In the cellular components group, 493 identified proteins and 82 DEPs were involved in cell, and 281 identified proteins and 50 DEPs were involved in macromolecular complex. Finally, in the molecular function group, 1,253 identified proteins and 200 DEPs were involved in catalytic activity, and 1072 identified proteins and 147 DEPs were involved in binding activity.

All identified proteins and DEPs were assorted according to their subcellular

localizations. In summary, 15 different subcellular components were identified, containing 1,142 chloroplast-localized proteins, 698 cytoplasm-localized proteins, and 366 nucleus-localized proteins (Fig. 2b). As for DEPs, only 10 different subcellular components were found, containing 218 chloroplast-localized DEPs comprising 52 up-regulated and 166 down-regulated DEPs, 82 cytoplasm-localized DEPs comprising 36 up-regulated and 46 down-regulated DEPs, and 24 nucleus-localized DEPs comprising 13 up-regulated and 11 down-regulated DEPs (Fig. 2c).

## Enrichment analysis of DEPs responsive to CWMV infection

In order to further explore the DEPs responsive to CWMV infection, enrichment analysis of 394 DEPs was performed respectively based on GO annotations, KEGG and protein domain. Among these 394 DEPs, 146 proteins were significantly up-regulated and 248 proteins were significantly down-regulated (Additional file 5: Fig. S2). A large number of up-regulated DEPs were mainly associated with metabolic process (74 proteins), catalytic activity (70 proteins) and binding (54 proteins) (Fig. 3a). For the down-regulated DEPs, metabolic process (147 proteins), catalytic activity (130 proteins) and cellular process (117 proteins) were mostly involved (Fig. 3b). For GO enrichment-based cluster analysis, DEPs involved in three groups were plotted. For the biological process group, DEPs were enriched in glycerol ether metabolic process, cell redox homeostasis, tetrapyrrole biosynthetic process, organic acid catabolic process and photosynthetic electron transport chain. For the molecular function group, the DEPs were enriched in protein disulfide oxidoreductase activity, cysteine-type endopeptidase activity, disulfide oxidoreductase activity, structural constituent of ribosome, histidinol

dehydrogenase activity, glycine dehydrogenase (decarboxylating) activity, peroxiredoxin activity and protochlorophyllide reductase activity. As for the cellular components group, DEPs were enriched in endoplasmic reticulum (Fig. 4). KEGG enrichment analysis showed that DEPs were closely related to Photosynthesis - antenna proteins(nta00196), MAPK signaling pathway – plant (nta04016), Glyoxylate and dicarboxylate metabolism (nta00630), Glycine, serine and threonine metabolism (nta00260), Porphyrin and chlorophyll metabolism (nta00860) and Carbon fixation in photosynthetic organisms (nta00710) (Fig. 5a). Protein enrichment analysis showed that DEPs were mainly enriched in Chlorophyll a/b binding protein domain, Peptidase C1A, propeptide, Cell division protein FtsZ, C-terminal, PsbQ-like domain, Aldolase-type TIM barrel, Thioredoxin domain, 30s ribosomal protein S13, C-terminal, Glutamate synthase, alpha subunit, C-terminal, Ribosomal protein S13-like, H2TH, Hydrophobic seed protein, Ribosomal protein L5, C-terminal, Peroxiredoxin, C-terminal, Ribosomal protein S5 domain 2-type fold, subgroup, Calreticulin/calnexin, P domain, Aquaporin-like, Thioredoxin-like fold, Glyceraldehyde 3-phosphate dehydrogenase, NAD(P) binding domain, Glyceraldehyde 3-phosphate dehydrogenase, catalytic domain, Alpha-D-phosphohexomutase, alpha/beta/alpha domain III and Alpha-D-phosphohexomutase, alpha/beta/alpha domain I (Fig. 5b).

## Identification of representative DEPs from three mostly enriched KEGG pathways

According to our proteomic data analysis, a total of 15 DEPs was involved in Photosynthesis - antenna proteins pathway, nine DEPs were involved in MAPK

signaling – plant pathway and 18 DEPs were involved in Glyoxylate and dicarboxylate metabolism pathway. Five representative proteins (P27491, A0A1S3Y974, A0A1S4DJQ0, A0A076L1Y1 and A0A1S4BSH6) from Photosynthesis - antenna proteins pathway, five representative proteins (P17514, A0A1S3XTH4, P24091, A0A1S3ZVW5 and A0A1S4DGP1) from MAPK signaling pathway – plant pathway and five representative proteins (A0A1S3YRT4, A0A1S3ZFE6, A0A1S3Y2X0, A0A1S3YYG2 and A0A1S4BAT9) from Glyoxylate and dicarboxylate metabolism pathway were illuminated for these three pathways were showing most significantly enriched (Table 1).

## Transcriptional level analysis for selected DEPs

To validate the changes at the protein level determined by proteomic analysis, nine genes encoding up-regulated DEPs and nine genes encoding down-regulated DEPs were selected for quantitative reverse transcription polymerase chain reaction (qRT-PCR). Among these selected genes encoding up-regulated DEPs, no significant change of *NbGCSH* expression was observed, and the expression level of the *NbPIP26b* was significantly decreased while the expression levels of other selected genes were increased under CWMV infection (Fig. 6b). Among these selected genes encoding down-regulated DEPs, the expression levels of seven selected genes were decreased (Fig. 6d) while there was no significant change in the expression of *NbSECR* gene, and the expression level of the *NbftsZ* gene was significantly increased. Although there are numerous studies reporting that gene transcription and protein abundance are not correlated, our results suggest that mRNA quantified of genes encoding most DEPs are

consistent with their protein expression levels. All basic information of selected DEPs is listed on Additional file 6: Table S4.

## ABA pathway is suppressed in CWMV-infected plants

More than half of representative selected DEPs in Table 1 were predicted to be localized in the chloroplast. Additionality, subcellular localization analysis showed that 35.62% up-regulated DEPs and 66.94% down-regulated DEPs were predicted to be localized in the chloroplast (Additional file 7: Figure S5). These results together suggested that CWMV invading probably altered the chloroplast structure and functions. Additionally, ABA synthesis are closely regulated by chloroplast machinery system [39]. ABA plays crucial roles in plant-virus interactions [40]. Label-free profiling analysis revealed that the expression levels of NbABA1 and the short-chain alcohol dehydrogenase (NbABA2) proteins were both significantly changed in CWMV-infected plants in comparison to that in mock plants (Figure 7a). qRT-PCR results showed that the mRNA expression levels of *NbABA1* and *NbABA2* were also significantly changed in CWMV-infected plants in comparison to that in mock plants (Figure 7b). Furthermore, qRT-PCR results displayed that the mRNA expression levels of ABA-biosynthetic genes (*NbNCED1*, *NbNCED3* and *NbAAO3*), ABA signaling transduction genes including (*NbPYL6* and *NbPYL9*), ABA-responsive genes (*NbRAB18* and *NbAGO4*) were significantly down-regulated in CWMV-infected plants compared with that in mock plants (Figure 7c). Additionally, further study showed that the contents of ABA in CWMV-infected plants were significantly decreased compared with that in mock plants (Figure 7d). These results together implied that ABA pathway was seriously interfered

in response to CWMV infection.

## Exogenous application of ABA induces plant resistance against CWMV infection

Because ABA signaling plays an important role in *N. benthamiana* under CWMV infection, we treated 4-leaf tobacco with ABA (100μM) or ABA inhibitor (NDGA)(10mM) and 0.2% EtOH (Mock). At 12 hours post-treatment, the pre-treated plants were inoculated with CWMV. The inoculated plants were grown inside a greenhouse for about four weeks. Results from this study showed that mock plants had typical symptoms of CWMV infection including stunting and chlorotic local lesions whereas ABA-treated tobacco showed CWMV symptoms were alleviated (Figure 8a). As we expected, NDGA-treated plants displayed that CWMV symptoms were promoted. In addition, accumulation levels of CWMV CP RNA as well as the CP protein were the highest in NDGA pre-treated plants and lowest in ABA pre-treated plants (Figure 8b and C). These data together suggested that ABA treatment can induce *N. benthamiana* defense against CWMV.

# Discussion

CWMV is transmitted by *P. graminis*, of which resting spores can survive in soils for over 10 years, displaying a durable threat to winter production in China [3, 41]. Besides, *P. graminis* is also the carrying vector transmitting *wheat yellow mosaic virus* (WYMV), together with CWMV, can co-infect wheat in China, resulting in more severe and quantity and quality losses [42, 43]. Thus, it is quite urgent to explore the molecular mechanisms in depth about how CWMV successfully establish an infection and how

243 the plant host respond to CWMV invade. In this study, comparative proteomic analysis
244 was conducted to gain a comprehensive whole-proteome information during CMWV
245 infection of *N. benthamiana*. The outcome of our work provides new insights to the
246 molecular basis of plant defense responsive to CWMV.
247 Pearson correlation coefficient are good (Fig. 1b). The relationship of protein mass and
248 coverage, and the distribution of identified peptides are both as expected (Fig. 1c-d).
249 These results demonstrate that the data analytical reproducibility and quality are
250 credible. A total of 394 DEPs was identified from *N. benthamiana* inoculated with
251 CWMV. Among these DEPs, 146 were up-regulated and 248 were down-regulated (Fig.
252 S2). It has been reported that Glyoxylate and dicarboxylate metabolism pathway mainly
253 enhance plants resistance against environmental stress by balancing metabolic
254 disorders and transferring energy [32, 33]. In this study, we also found that Glyoxylate
255 and dicarboxylate metabolism pathway was significantly enriched after CWMV
256 infected. Among these DEPs contains 18 proteins was characterized and their
257 expressions levels were significantly changed, which suggested CWMV infection
258 might destroy the host immune system by interfering Glyoxylate and dicarboxylate
259 metabolism pathway. The MAPK signaling pathway is deeply involved in the plant
260 growth and development, plant response to environmental stress and pathogenic
261 microorganism invasion [34]. Payne et al cloned two acidic endochitinase genes
262 encoding the pathogenesis-related proteins PR-P and PR-Q, and the expression of these
263 two proteins is induced by TMV infection [35]. In our study, the expression level of
264 acidic endochitinase Q from significantly enriched MAPK signaling pathway was up-

regulated over 48-fold by CWMV infection (Table 1), which indicated that MAPK signaling pathway played an important role in the response of *N. benthamiana* to CWMV infection. Plant RNA viral infection usually leads to leaf chlorosis, necrosis, plant stunting or other symptoms, and leaf chlorosis is often consistent with decreased photosynthetic activity of the chloroplast [36, 37]. The chlorophyll a/b proteins (CAB) from Photosynthesis - antenna proteins pathway are vital membrane proteins for the capture of light energy by combining with pigment molecules in photosynthesis [38]. Agree with this result, we also found a few chlorotic lesions appeared on the leaves of inoculated plants with CWMV (Fig. S1a). Furthermore, our data also showed that Photosynthesis - antenna proteins pathway was significantly enriched. Such as a series of CAB proteins were down-regulated (Table 1) and more than half of DEPs were predicted to located in the chloroplast under CWMV infection (Fig. 2c), which suggested that CWMV invasion probably altered the chloroplast structure and functions. In fact, lots of plant RNA viruses recruit the chloroplast membrane to facilitate their infection, and affect many chloroplast-related genes expression including photosynthesis-related genes [39-41]. Chloroplasts are the source of numerous pro-defense signals, and they are closely related to the initiation of effector-triggered immunity (ETI) [42-44]. More importantly, a series of key steps of ABA biosynthesis pathway occur in the chloroplast. The relationship between fungi or bacteria and ABA has been extensively studied, but the interaction between ABA and plant virus is still not well understood. Early study shows the TMV infection increase the ABA contents in tobacco plants [45]. AGO2 and AGO3 are reported to contribute to ABA-mediated

287 defense against *bamboo mosaic virus* (BaMV) [46]. A study in rice shows that ABA
288 treatment does increase susceptibility to RBSDV infection by suppressing the
289 jasmonate pathway and induction of ROS [47]. Besides, both ABA1 and ABA2 play
290 key roles in ABA synthesis and ABA1 functions in the chloroplast [48-50]. ABA1 and
291 ABA2 of the ABA pathway has been reported deeply involved in the viral accumulation
292 in *A. thaliana* [51]. Amino acid sequence analysis showed that *NbABA1* shared 96%
293 sequence identity with *Nicotiana tabacum* ABA1 (NtABA1) and a 69% sequence
294 identity with *Arabidopsis thaliana* ABA1 (AtABA1) (Additional file 8: Fig. S4).
295 *NbABA2* shared a 92% sequence identity with *N. tabacum* ABA2 (NtABA2) and a 66%
296 sequence identity with *A. thaliana* ABA2 (AtABA2) (Additional file 9: Fig. S5). We
297 silenced *NbABA1* and *NbABA2* respectively using *tobacco rattle virus* (TRV)-based
298 VIGS system. qRT-PCR data ensured that mRNA expression levels of *NbABA1* and
299 *NbABA2* were down-regulated (Fig. 9b). No significant phenotypic changes were
300 observed in *NbABA1*-silenced or *NbABA2*-silenced plants (Fig. 9a). Moreover, qPCR
301 results showed that the expression levels of ABA-responsive genes including *NbRAB18*
302 and *NbAGO4* were down-regulated in *NbABA1*-silenced or *NbABA2* -silenced plants,
303 compared to that in the control plants (Fig. 9c-d). In addition, silencing of *NbABA1* or
304 *NbABA2* significantly decreased the concentrations of ABA in *N. benthamiana* (Fig.
305 9e). These results, together with amino acid sequence analysis (Fig. S4 and S5),
306 confirmed that NbABA1 and NbABA2 were indeed involved in the ABA signaling
307 pathway. Silencing *ABA1* significantly increased CWMV accumulation (Fig. 9f) and
308 silencing *ABA2* also significantly enhanced CWMV accumulation (Fig. 9g). These data

also suggest that NbABA1 and NbABA2 paly positive regulators in response to CWMV infection. To investigate the detailed relationship between the ABA pathway and CWMV, qRT-PCR was performed and its results showed that the mRNA expression levels of ABA-biosynthetic genes including *NbNCED1*, *NbNCED3*, and *NbAAO3*, ABA-signal-transduction genes including *NbPYL6* and *NbPYL9* and ABA-responsive genes *NbRAB18* and *NbAGO4* were decreased under CWMV infection (Fig. 7c). These data, together with the decreasing of ABA contents in the CWMV-infected plants compared to mock plants (Fig. 7d), imply that CWMV infection truly suppress the ABA pathway by interfering the expression of ABA1 and ABA2.

In summary, our results identified several pathways seriously involved in the *N. benthamiana* responses to CWMV infection and we also explored the relationship between CWMV infection and ABA signaling pathway.

## Conclusions

CWMV leads to devastating damage to wheat production and its causing disease of winter wheat is diffcult to be controlled [52, 53]. Now breeding of resistant wheat is the most effective and economical countermeasure for prevention and control of CWMV causing disease. However, only a few cultivars are indentified to be resistant against CWMV[54]. In this study, a proteomic manner was employed to explore the proteomic changes of *N. benthamiana* under CWMV infection. A total of 394 DEPs were identified and characterized according to their annotations. Photosynthesis - antenna proteins, MAPK signaling – plant and Glyoxylate and dicarboxylate metabolism pathways were most significantly enriched with DEPs. CWMV infection did suppress

the ABA pathway in *N. benthamiana*. In summary, our results also laid a good foundation for providing antiviral candidate factors to cultivate resistant varieties.

# Methods

### Plant material and CWMV inoculation

*N. benthamiana* seeds were kindly provided by Prof. Yule Liu (Tsinghua University, Beijing) and grown inside a greenhouse at 22℃ with a 16/8 h (hours) (light/dark) photoperiod until four-leaf stage for CWMV inoculation. CWMV inoculation was performed as previously described with small modifications previously [31]. *A. tumefaciens* strain GV3101 carrying CWMV RNA1 and RNA2 genomes was prepared. The agrobacterium cultures were grown overnight, pelleted, re-suspended in an induction buffer (1M $MgCl_2$, 10mM MES, pH=5.6, and 100mM acetosyringone) and incubated for 3 h at room temperature prior to leaf infiltration. All inoculated plants were grown in a constant temperature incubator at 17℃ with a 14/10 h (light/dark) photoperiod. qRT-PCR and western blot were performed to confirm successful systemic infection at 14 days post CWMV inoculation (dpi). Samples were collected for further analysis.

### RNA extraction and quantitative reverse transcription polymerase chain reaction (qRT-PCR)

Total RNAs were isolated from prepared samples at 14 days post CWMV inoculation (dpi) using Trizol Reagent (Invitrogen, Carlsbad, CA, USA). First strand cDNA was

353 synthesized using a First Strand cDNA Synthesis Kit (TOYOBO, Kita-ku, Osaka,
354 Japan). qRT-PCR reaction was performed on an ABI7900HT Sequence Detection
355 System (Applied Biosystems, Foster City, CA, USA) with an AceQ qPCR SYBR Green
356 Master Mix (Vazyme, Nanjing, Jiangsu, China). Each treatment at least contains three
357 biological replicates, which at least owns three technical replicates each. Relative
358 expression levels of ABA related genes and CWMV CP were analyzed using the $2^{-\Delta\Delta C(t)}$
359 method as described [55]. Actin gene was referred as an internal reference. These
360 primers used in qRT-PCR are listed in Additional file 10: Table S5.
361
362 **Western blot**
363 Western blot assay was performed as described previously with small modifications [6,
364 31]. Collected samples were individually ground in liquid nitrogen and then
365 homogenized in a protein extraction buffer (Sigma-Aldrich, St. Louis, MO, USA)
366 supplemented with Protease Inhibitor Cocktail Tablets (Roche, 1 tablet/50mL buffer).
367 After 20 min centrifugation at 16,000 g at 4 °C, the supernatant was collected, boiled
368 for 10 min and proteins were separated in SDS-PAGE gels through electrophoresis
369 prior to transferring to nitrocellulose membranes (NC). The antibody specially
370 detecting CWMV CP was made in our laboratory.
371
372 **Protein extraction**
373 Protein extraction for LC-MS/MS was conducted mainly as described previously with
374 small modifications [56-58]. Samples powders were collected and ground individually

in liquid nitrogen. 0.1g sample powders were transferred into extraction buffer (200mM Tris-Cl, pH 7.4, 250mM sucrose, 1mM $MgCl_2$, 5mM KCl, 2mM PMSF, 10mM β -mercaptoethanol and 1× complete EDTA-free protease inhibitor) and then vortexed severely. The collection was incubated for 30 min at 25 °C. After centrifugation at 16,000 g for 20 min at 4°C, resulting supernatant was mixed with equal volume of buffered phenol (pH 8.0). The pellets were then dried using a Speed-Vacuum concentrator and then resuspended using solution buffer made up of 1× phosphate buffered saline (PBS) and 10× sodium dodecyl sulfate (SDS) (v/v, 3:4) and stored at -80°C. Protein concentration and quantification was conducted by RC DC™ Protein Assay (Bio-Rad).

**Protein digestion**

For trypsin digestion, protein samples were diluted five times by adding 100 mM Triethylamonium bicarbonat (TEAB). Trypsin was added into collection mixtures at a ratio of 1:50 (mass ratio, trypsin: protein) for digestion overnight. Then the digested collection mixtures were vacuum dried for further analysis.

**LC-MS/MS analysis**

The collection mixtures were dissolved in solvent A (0.1%formic acid), directly loaded into a home-made reversed-phase analytical column (15-cm length, 75 μm i.d.). The gradient was made up of an increase from 6% to 23% solvent B (0.1% formic acid in 98% acetonitrile) over 25 min, 23% to 35% in 8 min and climbing to 80% in 3 min then

holding at 80% for 3 min, all at a constant flow rate of 400 nL/min on an EASY-nLC 1000 UPLC system. These peptides were subjected to NSI source followed by tandem mass spectrometry (MS/MS) in Q Exactive$^{TM}$ Plus (Thermo) coupled online to the UPLC. The electrospray voltage applied was 2.0 kV. The m/z scan range was 350 to 1800 for full scan, and intact peptides were detected in the Orbitrap at a resolution of 70,000. Peptides were then selected for MS/MS using NCE setting as 28 and the fragments were detected in the Orbitrap at a resolution of 17,500. A data-dependent procedure that alternated between one MS scan followed by 20 MS/MS scans with 15s dynamic exclusion. Automatic gain control (AGC) was set at 5E4. Fixed first mass was set as 100 m/z.

**Database search**

The resulting MS/MS data were processed using Maxquant search engine (v.1.5.2.8). Tandem mass spectra were searched against UniProt *Nicotiana tabacum* database (73,605 sequences total) concatenated with reverse decoy database. Trypsin/P was specified as cleavage enzyme allowing up to 2 missing cleavages. The mass tolerance for precursor ions was set as 20 ppm in First search and 5 ppm in Main search, and the mass tolerance for fragment ions was set as 0.02 Da. Carbamidomethyl on Cys was specified as fixed modification and oxidation on Met was specified as variable modifications. FDR was adjusted to < 1% and minimum score for peptides was set > 40.

**Protein annotation**

Gene Ontology (GO) annotation was obtained for the protein sequences from the UniProt-GOA database (www.http://www.ebi.ac.uk/GOA/). Firstly, the identified protein's ID was converted to a UniProt ID and then mapped to GO IDs by protein ID. For identified proteins that were not annotated in the UniProt-GOA database, the InterProScan software (v.5.14-53.0) (www.http://www.ebi.ac.uk/interpro) was used to annotate the protein's GO function. Then, the proteins were classified by Gene Ontology annotation according to three groups: biological process, cellular component, and molecular function.

The proteins in eukaryotic cells, according to different membrane structure which they bind, are localized in various cellular organelles. The main subcellular localization of eukaryotic cells includes extracellular, cytoplasm, nucleus, mitochondria, Golgi apparatus, endoplasmic reticulum, peroxisomes, vacuole, cytoskeleton, nucleoplasm, nuclear matrix and ribosome. We used Wolfpsort (v.0.2) (www.http://www.genscript.com/psort/wolf_psort.html), a subcellular localization predication software. Wolfpsort is an updated version of PSORT/PSORT II, which is for the prediction of eukaryotic sequences.

Kyoto Encyclopedia of Genes and Genomes (KEGG) database was used for pathway annotation. Firstly, using KEGG online service tools KAAS to annotated protein's KEGG database description. Then mapping the annotation result on the KEGG pathway database using KEGG online service tools KEGG mapper.

Identified proteins domain functional description were annotated by InterProScan (a

sequence analysis application) based on protein sequence alignment method, and the InterPro domain database was used. InterPro (http://www.ebi.ac.uk/interpro/) is a database that integrates diverse information about protein families, domains and functional sites, and makes it freely available to the public via Web-based interfaces and services. Central to the database are diagnostic models, known as signatures, against which protein sequences can be searched to determine their potential function. InterPro has utility in the large-scale analysis of whole genomes and meta-genomes, as well as in characterizing individual protein sequences.

**Functional enrichment analysis**

Proteins were classified by GO annotation into three categories: biological process, cellular compartment and molecular function. For each category, a two-tailed Fisher's exact test was employed to test the enrichment of the DEPs against all identified proteins. The GO with a corrected $p$ values < 0.05 is considered significant.

Encyclopedia of Genes and Genomes (KEGG) database was used to identify enriched pathways by a two-tailed Fisher's exact test to test the enrichment of the DEPs against all identified proteins. The pathway with a corrected $p$ value < 0.05 was considered significant. These pathways were classified into hierarchical categories according to the KEGG website.

For each category proteins, InterPro (a resource that provides functional analysis of protein sequences by classifying them into families and predicting the presence of domains and important sites) database was researched and a two-tailed Fisher's exact

test was employed to test the enrichment of the DEPs against all identified proteins. Protein domains with a $p$ value < 0.05 were considered significant.

**ABA and ABA inhibitor treatments (NDGA)**

Abscisic acid (ABA, Sigma-Aldrich, St. Louis, MO, USA) was dissolved with 0.2 % ethanol till 100 μM. NDGA (Sigma-Aldrich, St. Louis, MO, USA), targeting 9-*cis*-epoxycarotenoid dioxygenase was dissolved with 0.2 % ethanol till 10 mM. *N. benthamiana* plants were applied with 100 μM ABA solution or 10 mM NDGA solution and 0.2 % ethanol solution as a control (Mock). All solutions were applied into the adaxial and abaxial sides of leaves until solution drops began to run off leaves. 12 h later, pre-treated *N. benthamiana* leaves were inoculated with CWMV.

**Analysis of ABA contents**

Samples were collected from assayed plants for ABA extraction as described previously [59]. Collected samples were then ground in liquid nitrogen, and then mixed individually (200 mg leaf powder per sample) with $^{2}H_5$-ABA 45 pmol. Two milliliter methanol was added to each sample, mixed, and the mixture was incubated overnight at -20 ℃. After 20 min centrifugation at 160,000g at 4 ℃, supernatant of each sample was collected and dried under the nitrogen gas. The pellets were individually dissolved in 1 mL 5 % ammonia solution and purified using the Oasis MAX SPE columns as instructed (Waters, Milford, MA, USA). The eluted ABA was dried again under nitrogen gas, dissolved in 200 μL water/methanol mixture (20:80, v/v), and then

analyzed by Ultrahigh Liquid Chromatography-triple Quadrupole Mass Spectrometry (UPLC-MS/MS). Three independent biological replicates were analyzed for each.

**Plasmids construction**

Partial length *NbABA1*and *NbABA2* gene sequences were PCR amplified. These PCR products were then digested with *BamH*I *and Sma*I (New England Biolabs, Ipswich, MA, USA) restriction enzymes. These digested PCR products cloned individually into *Tobacco rattle virus* (TRV)-based pTRV2 to generate pTRV2:NbABA1 and pTRV2:NbABA2 vectors. PCR products used for plasmids construction were all generated using KOD DNA polymerase (TOYOBO, Kita-ku, Osaka, Japan).

**Virus-induced gene silencing (VIGS)**

*Tobacco rattle virus* (TRV)-based VIGS system in *N. benthamiana* was described as previously with small modifications [60]. pTRV2:NbABA1and pTRV2:NbABA2 vectors were individually transformed into *A. tumefaciens* strain GV3101 by electroporation. The agrobacterium cultures and *A. tumefaciens* strain GV3101 containing TRV RNA1 were grown overnight, pelleted, re-suspended in an induction buffer and incubated for 3 h at room temperature prior to leaf co-infiltration. Infiltrated leaves were collected at 7 days post agro-infiltration (dpai) and examined using qRT-PCR to confirm the silencing of target-genes.

# Figure legends

**Fig. 1** Experimental strategy for quantitative proteome analysis and quality control validation of MS data. **a** Proteins were extracted from three biological replicates for each sample group. All protein samples were digested with trypsin and analyzed by LC/MS. **b** Pearson's correlations. **c** mass delta of all identified peptides. **d** length distribution of all identified peptides.

**Fig. 2** Classifications of identified proteins and DEPs. **a** GO analysis of all identified proteins and DEPs. **b** Subcellular locations analysis of all identified proteins. **c** Subcellular locations analysis of all DEPs.

**Fig. 3** GO analysis of up-regulated and down-regulated DEPs. **a** GO analysis of up-regulated DEPs. **b** GO analysis of down-regulated DEPs.

**Fig. 4** GO enrichment analysis of DEPs. Significantly enriched GO terms of all DEPs.

**Fig. 5** Enrichment analysis of DEPs. **a** Significantly enriched KEGG terms of all DEPs. **b** Significantly enriched protein domain terms of all DEPs.

**Fig. 6** Validation of *N. benthamiana* selected genes expression. **a** Nine up-regulated DEPs selected. **b** qRT-PCR showing genes encoding nine up-regulated DEPs selected. Each mean ± SD was from three biological replicates and each replicate had three technical replicates. **, $p< 0.01$; ns, not significant determined by the Student's *t*-test. **c** Nine down-regulated DAPs selected. **d** qRT-PCR showing genes encoding nine down-regulated DAPs selected. Each mean ± SD was from three biological replicates and each replicate had three technical replicates. **, $p< 0.01$; ns, not significant determined by the Student's *t*-test.

**Fig. 7** Effects of CWMV infection on the ABA pathway. **a** Proteins (ABA1and ABA2) involved in the ABA signaling pathway that significantly changed responsive to CWMV infection. **b** qRT-PCR data showing the expression of *NbABA1* and *NbABA2* under CWMV infection. **c** qRT-PCR data showing the expression of ABA-pathway genes under CWMV infection. Each mean ± SD was from three biological replicates, and each replicate had three technical replicates. **, $p< 0.01$ determined by the Student's *t*-test. **d** detection of endogenous ABA production in mock and CWMV-infected plants. Each mean ± SD was from three biological replicates, and each replicate had three technical replicates. **, $p< 0.01$ determined by the Student's *t*-test.

**Fig.8** Effects of ABA and its inhibitor application on CWMV infection in *N. benthamiana*. **a** Phenotype of *N. benthamiana* treated with 100 μM ABA or 10 mM NDGA or 0.2% EtOH (mock) followed CWMV inoculation at 21 dpi. **b** qRT-PCR results showing the mRNA expression of CWMV CP in pre-treated plants. Each mean ± SD was from three biological replicates, and each replicate had three technical replicates. **, $p< 0.01$ determined by the Student's *t*-test. **c** Western blot analyses of CWMV CP protein accumulation in the ABA or NDGA pre-treated CMWV-inoculated plants. CBB-stained loadings are shown at the bottom of the figure.

**Fig.9** Effects of silencing *NbABA1* or *NbABA2* on CWMV CP accumulation. **a** Phenotypes of *NbABA1*-silenced and *NbABA2*-silenced plant. Photograph taken at 7 dpai. **b** qRT-PCR showing mRNA expression of *NbABA1* and *NbABA2*. Each mean ± SD is from three biological replicates, and each replicate had three technical replicates. **, $p<0.01$ determined by the Student's *t*-test. **c** qRT-PCR showing mRNA expression

of *NbRAB18* and *NbAGO4* in *NbABA1*-silenced plants. **d** qRT-PCR showing mRNA expression of *NbRAB18* and *NbAGO4* in *NbABA2*-silenced plants. Each mean ± SD was from three biological replicates and each replicate had three technical replicates. **, $p< 0.01$ determined by the Student's *t*-test. **e** detection of endogenous ABA production in Control and *NbABA1*-silenced or *NbABA2*-silenced plants. Three independent biological replicates were analyzed for each treatment. **, $p< 0.01$ determined by the Student's *t*-test. **f** qRT-PCR showing mRNA **(left)** and western blot assay showing protein **(right)** expression of CWMV CP respectively in *NbABA1*-slienced plants. **g** qRT-PCR showing mRNA **(left)** and western blot assay showing protein **(right)** expression of CWMV CP respectively in *NbABA2*-slienced plants. Each mean ± SD is from three biological replicates and each replicate had three technical replicates. **, $p< 0.01$ and was determined by the Student's *t*-test. CBB-stained loadings are shown in the bottom of the figure.

# Tables

**Table 1** Identification of selected DEPs from significantly changed pathways through KEGG enrichment analysis

| Protein accession | Protein description | Infected/Mock Ratio | Infected/Mock *P* value | Subcellular localization |
|---|---|---|---|---|
| Photosynthesis - antenna proteins | | | | |
| P27491 | Chlorophyll a-b binding protein 7 | 0.132 | 0.0000002020 | chloroplast |
| A0A1S3Y974 | Chlorophyll a-b binding protein | 0.168 | 0.000098992 | chloroplast |
| A0A1S4DJQ0 | Chlorophyll a-b binding protein | 0.191 | 0.0000157343 | chloroplast |
| A0A076L1Y1 | Chlorophyll a-b binding protein | 0.252 | 0.00004201 | chloroplast |
| A0A1S4BSH6 | Chlorophyll a-b binding protein | 0.256 | 0.00148307 | chloroplast |
| MAPK signaling pathway – plant | | | | |
| P17514 | Acidic endochitinase Q | 48.587 | 0.008995 | nucleus |
| A0A1S3XTH4 | Basic form of pathogenesis-related protein 1-like | 2.983 | 0.000075712 | chloroplast |
| P24091 | Endochitinase B | 2.863 | 0.000121412 | extracellular |
| A0A1S3ZVW5 | Basic endochitinase-like | 2.264 | 0.0138624 | chloroplast |
| A0A1S4DGP1 | Nucleoside diphosphate kinase | 0.472 | 0.0094373 | chloroplast |
| Glyoxylate and dicarboxylate metabolism | | | | |
| A0A1S3YRT4 | Glycine cleavage system H protein | 4.204 | 0.0021605 | mitochondria |
| A0A1S3ZFE6 | Catalase | 1.53 | 0.0082996 | cytoplasm |
| A0A1S3Y2X0 | Serine hydroxymethyltransferase | 0.43 | 0.0047004 | mitochondria |
| A0A1S3YYG2 | Glycine cleavage system P protein | 0.444 | 0.00091813 | mitochondria |
| A0A1S4BAT9 | Glutamate--glyoxylate aminotransferase 2 | 0.531 | 0.000020175 | cytoplasm |

## Supplementary information

**Additional file 1: Figure S1.** Samples inoculated with CWMV. **a** Left: mock (*N. benthamiana* inoculated with GV3101), right: *N. benthamiana* plant by 14 dpi. **b** PCR assay for detecting CWMV *CP* and *MP* gene. Lanes 1 to 3 below mock, samples were prepared from *N. benthamiana*. Lanes1 to 3 below CWMV-infected, samples were prepared from *N. benthamiana* by 14 dpi. PC, positive control. NC, negative control. **c** western blot assay for detecting CWMV CP protein. Lanes 1 to 3 below mock, samples were prepared from *N. benthamiana*. Lanes 1 to 3 below CWMV-infected, samples were prepared from *N. benthamiana* by 14 dpi. Coomassie brilliant blue (CBB)-stained loadings are shown in the bottom of the Figure.

**Additional file 2: Table S1.** Detailed information of identified peptides.

**Additional file 3: Table S2.** Detailed information of all identified proteins.

**Additional file 4: Table S3.** Detailed information of all DEPs.

**Additional file 5: Figure S2.** Numbers of up-regulated and down- regulated DEPs in CWMV-infected plants compared to that in mock plants.

**Additional file 6: Table S4.** Basic information of selected DEPs for qRT-PCR validation.

**Additional file 7: Figure S3.** Subcellular location of up-regulated and down-regulated DEPs. **a** Subcellular location of up-regulated DEPs. **b** Subcellular location of down-regulated DEPs.

**Additional file 8: Figure S4.** Multiple sequence alignment result. Amino acid sequence of Polypeptide (NbABA1) was aligned with sequences of *N. tabacum*, and *A. thaliana*

ABA1 sequences using DNAMAN software.

**Additional file 9: Figure S5.** Multiple sequence alignment result. Amino acid sequence of Polypeptide (NbABA2) was aligned with sequences of *N. tabacum*, and *A. thaliana* ABA2 sequences using DNAMAN software.

**Additional file 10: Table S5.** Primers used in this study.

**Additional file 11:** Full length image of Figure S1b, Figure S1c, Figure 8c, Figure 9f right and Figure 9g right.

## Abbreviations

CWMV: *Chinese wheat mosaic virus*; *P. graminis*: *Polymyxa graminis*; MS:mass spectrometry; DEPs: differentially expressed proteins; *N. benthamiana*: *Nicotiana benthamiana*; ABA: abscisic acid; ABA1: zeaxanthin epoxidase; ABA2:xanthoxin dehydrogenase.

## Declarations

### Ethics approval and consent to participate

Not applicable.

### Consent for publication

Not applicable.

### Competing interests

The authors declare that they have no competing interests.

## Availability of data and materials

All data generated or analyzed in this study are included in this article and its supplementary materials. All raw mass spectrometry (MS) data files has been deposited and can be access on the proteomeXchange with the dataset identifier PXD017593 (https://www.ebi.ac.uk/pride/profile/hnndhelong2).


## Funding

This work was supported by National Key R&D Plan in China (2018YFD0200507), Natural Science Foundation of Ningbo City (2019A610415), National Key R&D Plan in China (2017YFD-0201701, 2018YFD0200408), and China Agriculture Research System from the Ministry of Agriculture of the P.R. China (CARS-03), and National Key Project for Research on Transgenic Biology (2016ZX08002-001), and K.C. Wong Magna Funding Ningbo University. These funders had no role in the design of the study and collection, analysis, and interpretation of data and in writing this manuscript.


## Authors' contributions

HL and YJ conceived the project and designed the experiments; HL, JP, CX, ZTY, ZKL and LP carried out the experiments; HL and YJ analyzed the results and wrote the manuscript; YJ and CJP revised the manuscript. All authors read and approved the final manuscript.

**Acknowledgements**

We thank Prof. Yule Liu for providing *N. benthamiana* seeds.

# References

1. Sanfaçon H. Grand challenge in plant virology: understanding the impact of plant viruses in model plants, in agricultural crops, and in complex ecosystems. Front Micbiol.2017; 8,860.
2. Alexander HM, Mauck KE, Whitfield AE, Garrett KA, Malmstrom CM. Plant-virus interactions and the agro-ecological interface. Eur J Plant Pathol. 2014; 138(3):529-547.
3. Wang A. Dissecting the Molecular Network of Virus-Plant Interactions: The Complex Roles of Host Factors. Annu Rev Phytopathol. 2015; 53(1):45-66.
4. Garciaruiz H. Host factors against plant viruses. Mol Plant Pathol. 2019; 20(11):1588-1601.
5. Lian J, Qin Q, Yu W, Pu Y, Liu L, Xing W, Ji S, Wu J, Wei C, Ding B. *Rice Dwarf Virus* P2 Protein Hijacks Auxin Signaling by Directly Targeting the Rice OsIAA10 Protein, Enhancing Viral Infection and Disease Development. Plos Pathog.2016; 12(9):e1005847.
6. He L, Chen X, Yang J, Zhang T, Li J, Zhang S, Zhong K, Zhang H, Chen JP, Yang J. *Rice Black-Streaked Dwarf Virus* encoded P5-1 Regulates the Ubiquitination Activity of SCF E3 Ligases and Inhibits Jasmonate Signaling to Benefit Its Infection in Rice. New Phytol. 2020; 225(2):896-912.

7. Meena RP, Sendhil R, Tripathi S, Chander S, Chhokar R, Sharma R. Hydro-priming of seed improves the water use efficiency, grain yield and net economic return of wheat under different moisture regimes.Sarrc Journal of Agricul. 2013; 11(2):149-159.

8. Foods FS. What Do People Eat. FAO*:* Rome*,* Italy 2017.

9. GUO LM, He J, Li J, CHEN JP, ZHANG HM. *Chinese wheat mosaic virus*: A long-term threat to wheat in China. J Integr Agr. 2019; 18(4):821-829.

10. King AM, Lefkowitz E, Adams MJ, Carstens EB. Virus taxonomy: ninth report of the International Committee on Taxonomy of Viruses, VOL. 9.Elsevier, 2011.

11. Ye Y, Gong Z.Cloning, Expression and Identification of Matrix Protein Gene of Wheat Rosette Stunt Virus (WRSV). Sheng wu hua xue yu sheng wu wu li xue bao Acta biochimica et biophysica Sinica. 1998; 30(5):520-524.

12. Kanyuka K, Ward E, Adams MJ. *Polymyxa graminis* and the cereal viruses it transmits: a research challenge. Mol Plant Pathol. 2003; 4(5):393-406.

13. Chen J. Occurrence of fungally transmitted wheat mosaic viruses in China. Ann appl biol. 1993; 123(1):55-61.

14. Adams MJ, Antoniw JF, Kreuze J. Virgaviridae: a new family of rod-shaped plant viruses. Arch virol. 2009; 154(12):1967-1972.

15. Diao A, Chen J, Ye R, Zheng T, Yu S, Antoniw J, Adams M. Complete sequence and genome properties of *Chinese wheat mosaic virus*, a new furovirus from China. J Gen Virol. 1999; 80(5):1141-1145.

16. Ye R, Zheng T, Chen J, Diao A, Adams M, Yu S, Antoniw J. Characterisation

685 and partial sequence of a new furovirus of wheat in China. Plant pathol. 1999;
686 48(3):379-387.
687 17. Yang J, Chen J, Jiang H, Zhao Q, Adams M. Sequence of a second isolate of
688 Chinese wheat mosaic furovirus. J of phytopathol. 2001; 149(3):135-140.
689 18. Andika IB, Zheng S, Tan Z, Sun L, Kondo H, Zhou X, Chen J. Endoplasmic
690 reticulum export and vesicle formation of the movement protein of *Chinese*
691 *wheat mosaic virus* are regulated by two transmembrane domains and depend
692 on the secretory pathway. Virol. 2013; 435(2):493-503.
693 19. Sun L, Andika IB, Shen J, Yang D, Chen J. The CUG-initiated larger form coat
694 protein of *Chinese wheat mosaic virus* binds to the cysteine-rich RNA silencing
695 suppressor. Virus Res. 2013; 177(1):66-74.
696 20. Sun L, Andika IB, Kondo H, Chen J. Identification of the amino acid residues
697 and domains in the cysteine-rich protein of *Chinese wheat mosaic virus* that are
698 important for RNA silencing suppression and subcellular localization. Mol Plant
699 Pathol. 2013; 14(3):265-278.
700 21. Andika IB, Sun L, Xiang R, Li J, Chen J. Root-specific role for *Nicotiana*
701 *benthamiana* RDR6 in the inhibition of *Chinese wheat mosaic virus*
702 accumulation at higher temperatures. Mol Plant Microbe In. 2013; 26(10):1165-
703 1175.
704 22. Yang J, Zhang F, Cai NJ, Wu N, Chen X, Li J, Meng XF, Zhu TQ, Chen JP,
705 Zhang HM. A furoviral replicase recruits host HSP70 to membranes for viral
706 RNA replication. Sci Rep-UK. 2017;7(1):1-15.

707 23. Yang J, Zhang T, Li J, Wu N, Wu G, Yang J, Chen X, He L, Chen JP. *Chinese*
708 *wheat mosaic virus*-derived vsiRNA-20 can regulate virus infection in wheat
709 through inhibition of vacuolar-(H+)-PPase induced cell death. New Phytol.
710 2019.
711 24. Fu S, Xu Y, Li C, Li Y, Wu J, Zhou X. *Rice Stripe Virus* Interferes with S-
712 acylation of Remorin and Induces Its Autophagic Degradation to Facilitate
713 Virus Infection. Mol Plant. 2017; 11(2):269-287.
714 25. Yue R, Lu C, Han X, Guo S, Yan S, Liu L, Fu X, Chen N, Guo X, Chi H.
715 Comparative proteomic analysis of maize (Zea mays L.) seedlings under *rice*
716 *black-streaked dwarf virus* infection. Bmc Plant Biol. 2018; 18(1):191.
717 26. Dang M, Cheng Q, Hu Y, Wu J, Zhou X, Qian Y. Proteomic Changes during
718 MCMV Infection Revealed by iTRAQ Quantitative Proteomic Analysis in
719 Maize. In J Mol Sci. 2019; 21(1):35.
720 27. Jiang S, Lu Y, Li K, Lin L, Chen J. Heat shock protein 70 is necessary for *Rice*
721 *stripe virus* infection in plants. Mol Plant Pathol. 2014; 15(9):907-917.
722 28. Bombarely A, Rosli HG, Vrebalov J, Moffett P, Mueller LA, Martin GB. A Draft
723 Genome Sequence of *Nicotiana benthamiana* to Enhance Molecular Plant-
724 Microbe Biology Research. Mol Plant Microbe In. 2012; 25(12):1523-1530.
725 29. Yang M, Zhang Y, Xie X, Yue N, Li D. *Barley Stripe Mosaic Viru*s γb Protein
726 Subverts Autophagy to Promote Viral Infection by Disrupting the ATG7-ATG8
727 Interaction. Plant Cell. 2018; 30(7) 00122-02018.
728 30. Goodin MM, Zaitlin D, Naidu RA, Lommel SA. *Nicotiana benthamiana*: its

729 history and future as a model for plant–pathogen interactions. Mol Plant
730 Microbe In. 2008; 21(8):1015-1026.
731 31. Yang J, Zhang F, Xie L, Song XJ, Li J, Chen JP, Zhang HM. Functional
732 identification of two minor capsid proteins from *Chinese wheat mosaic virus*
733 using its infectious full-length cDNA clones. J Gen Virol. 2016; 97(9):2441-
734 2450.
735 32. Chen T, Zhang L, Shang H, Liu S, Peng J, Gong W, Shi Y, Zhang S, Li J, Gong
736 J. iTRAQ-Based Quantitative Proteomic Analysis of Cotton Roots and Leaves
737 Reveals Pathways Associated with Salt Stress. PloS One. 2016; 11(2):e25131.
738 33. Zhao X, Chen Z, Leng P, Hu Z: iTRAQ-based quantitative proteomic analysis
739 of the response of *Hylotelephium erythrostictum* leaves to salt stress. Sci
740 Horticul. 2020; 264:109190.
741 34. Meng X, Zhang S. MAPK cascades in plant disease resistance signaling. Annu
742 Re Phytopathol. 2013; 51(1):245-266.
743 35. Payne G, Ahl P, Moyer M, Harper A, Beck J, Meins F, Ryals J. Isolation of
744 complementary DNA clones encoding pathogenesis-related proteins P and Q,
745 two acidic chitinases from tobacco. P Natl Aca Sci USA.1990; 87(1):98-102.
746 36. Zhao J, Xu J, Chen B, Cui W, Zhou Z, Song X, Chen Z, Zheng H, Lin L, Peng
747 J. Characterization of Proteins Involved in Chloroplast Targeting Disturbed by
748 *Rice Stripe Virus* by Novel Protoplast–Chloroplast Proteomics. Int J Mol Sci.
749 2019; 20(2):253.
750 37. Bhor SA, Tateda C, Mochizuki T, Sekine KT, Yaeno T, Yamaoka N, Nishiguchi

751 M, Kobayashi K. Inducible transgenic tobacco system to study the mechanisms
752 underlying chlorosis mediated by the silencing of chloroplast heat shock protein
753 90. Virus Disease 2017; 28(1):81-92.
754 38. Green BR, Durnford DG. The chlorophyll-carotenoid proteins of oxygenic
755 photosynthesis. Annu Rev Plant Physiol Plant Mol Biol. 1996; 47:685-714.
756 39. Mochizuki T, Ogata Y, Hirata Y, Ohki ST. Quantitative transcriptional changes
757 associated with chlorosis severity in mosaic leaves of tobacco plants infected
758 with C ucumber mosaic virus. Mol Plant Pathol. 2014; 15(3):242-254.
759 40. Postnikova OA, Nemchinov LG. Comparative analysis of microarray data in
760 *Arabidopsis* transcriptome during compatible interactions with plant viruses.
761 Virol J. 2012; 9(1):101.
762 41. Wei T, Huang TS, McNeil J, Laliberté JF, Hong J, Nelson RS, Wang A.
763 Sequential recruitment of the endoplasmic reticulum and chloroplasts for plant
764 potyvirus replication. J Virol.2010; 84(2):799-809.
765 42. Alazem M, Lin NS. Roles of plant hormones in the regulation of host–virus
766 interactions. Mol Plant Pathol. 2015; 16(5):529-540.
767 43. Ding X, Jimenez-Gongora T, Krenz B, Lozano-Duran R. Chloroplast clustering
768 around the nucleus is a general response to pathogen perception in *Nicotiana*
769 *benthamiana*. Mol Plant Pathol. 2019; 20(9):1298-1306.
770 44. Bhattacharyya D, Chakraborty S. Chloroplast: the Trojan horse in plant–virus
771 interaction. Mol Plant Pathol. 2018; 19(2):504-518.
772 45. Whenham R, Fraser R, Brown L, Payne J. *Tobacco mosaic virus* induced

773 increase in abscisic-acid concentration in tobacco leaves. Planta. 1986;
774 168(4):592-598.
775 46. Alazem M, He MH, Moffett P, Lin NS. Abscisic acid induces resistance against
776 *bamboo mosaic virus* through Argonaute 2 and 3. Plant Physiol. 2017;
777 174(1):339-355.
778 47. Xie K, Li L, Zhang H, Wang R, Tan X, He Y, Hong G, Li J, Ming F, Yao X.
779 Abscisic acid negatively modulates plant defence against *rice black-streaked*
780 *dwarf virus* infection by suppressing the jasmonate pathway and regulating
781 reactive oxygen species levels in rice. Plant Cell Environ. 2018; 41(10):2504-
782 2514.
783 48. Marin E, Nussaume L, Quesada A, Gonneau M, Sotta B, Hugueney P, Frey A,
784 Marion-Poll A. Molecular identification of *zeaxanthin epoxidase* of *Nicotiana*
785 *plumbaginifolia*, a gene involved in abscisic acid biosynthesis and
786 corresponding to the ABA locus of *Arabidopsis thaliana*. EMBO J. 1996;
787 15(10):2331-2342.
788 49. Audran C, Borel C, Frey A, Sotta B, Meyer C, Simonneau T, Marion Poll A.
789 Expression studies of the *zeaxanthin epoxidase* gene in *Nicotiana*
790 *plumbaginifolia*. Plant Physiol. 1998; 118(3):1021-1028.
791 50. González Guzmán M, Apostolova N, Bellés JM, Barrero JM, Piqueras P, Ponce
792 MR, Micol JL, Serrano R, Rodríguez PL. The short-chain alcohol
793 dehydrogenase ABA2 catalyzes the conversion of xanthoxin to abscisic
794 aldehyde. Plant Cell. 2002; 14(8):1833-1846.

795 51. Alazem M, Lin KY, Lin NS. The abscisic acid pathway has multifaceted effects
796 on the accumulation of *Bamboo mosaic virus*. Mol Plant Microbe In. 2014;
797 27(2):177-189.
798 52. Adams M. Transmission of plant viruses by fungi. Ann appl biol. 1991;
799 118(2):479-492.
800 53. Shirako Y, Suzuki N, French RC. Similarity and divergence among viruses in
801 the genus *Furovirus*. Virol. 2000; 270(1):201-207.
802 54. Yang JP, Chen JP, Cheng Y, Chen J, Jiang HM, Liu Q, Yang KS, Xu H, Adams
803 MJ. Responses of some American, European and Japanese wheat cultivars to
804 soil-borne wheat viruses in China. Agr Sci China. 2002; 1(10):1141-1150.
805 55. Livak K, Schmittgen T. Analysis of Relative Gene Expression Data Using Real-
806 Time Quantitative PCR and the $2^{-\triangle\triangle Ct}$ Method. Methods. 2000, 25(4).
807 56. Shen Z, Li P, Ni RJ, Ritchie M, Wang BC: Label-free Quantitative Proteomics
808 Analysis of Etiolated Maize Seedling Leaves during Greening. Mol Cell
809 Proteomics. 2009; 8(11):2443-2460.
810 57. Komatsu S, Han C, Nanjo Y, Yang P. Label-Free Quantitative Proteomic
811 Analysis of Abscisic Acid Effect in Early-Stage Soybean under Flooding. J+ of
812 Proteome Res. 2013; 12(11):4769.
813 58. Zhu W, Smith JW, Huang CM. Mass spectrometry-based label-free quantitative
814 proteomics.J Biomed Biotechnol. 2010; 3(11):01-06.
815 59. Fu J, Chu J, Sun X, Wang J, Yan C. Simple, Rapid, and Simultaneous Assay of
816 Multiple Carboxyl Containing Phytohormones in Wounded Tomatoes by

817 UPLC-MS/MS Using Single SPE Purification and Isotope Dilution. Anal Sci.
818 2012; 28(11):1081-1087.
819 60. Liu Y, Schiff M, Dinesh-Kumar S. Virus-induced gene silencing in tomato. Plant
820 J. 2002; 31(6):777-786.
821
822

# Figures

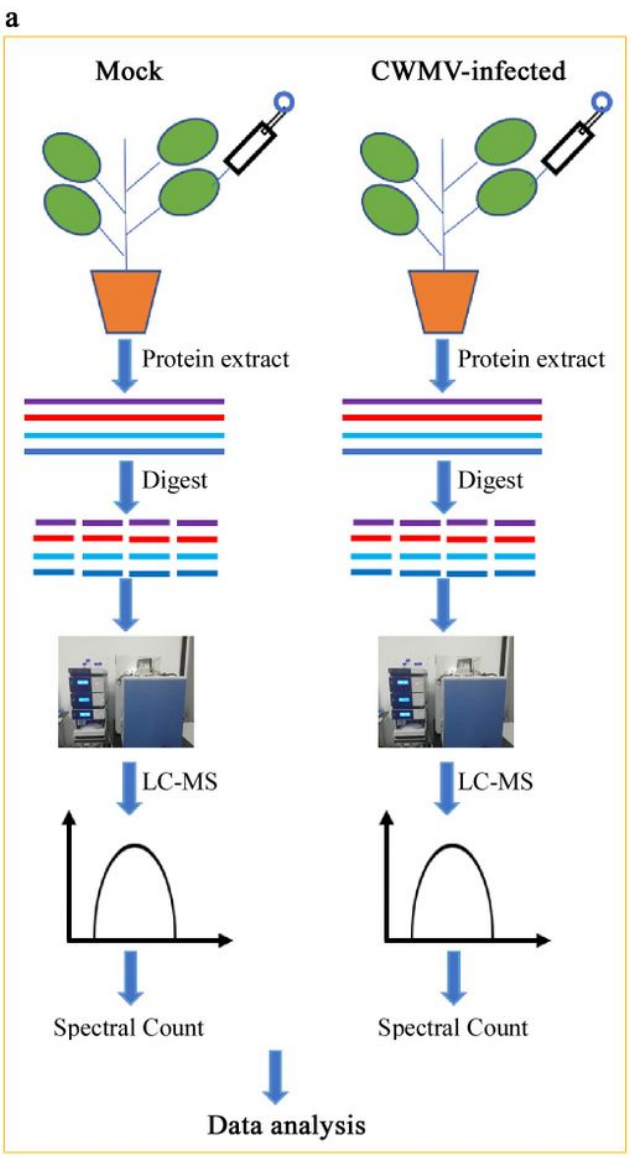


b

| Pearson's correlation of quantitation | | | | | | |
|---|---|---|---|---|---|---|
| | Mock1 | Mock2 | Mock3 | CWMV-infected1 | CWMV-infected2 | CWMV-infected3 |
| Mock1 | 1.00 | 0.96 | 0.97 | -0.92 | -0.93 | -0.93 |
| Mock2 | 0.96 | 1.00 | 0.96 | -0.96 | -0.92 | -0.95 |
| Mock3 | 0.97 | 0.96 | 1.00 | -0.93 | -0.89 | -0.89 |
| CWMV-infected1 | -0.92 | -0.96 | -0.93 | 1.00 | 0.92 | 0.95 |
| CWMV-infected2 | -0.93 | -0.92 | -0.89 | 0.92 | 1.00 | 0.91 |
| CWMV-infected3 | -0.93 | -0.95 | -0.89 | 0.95 | 0.91 | 1.00 |

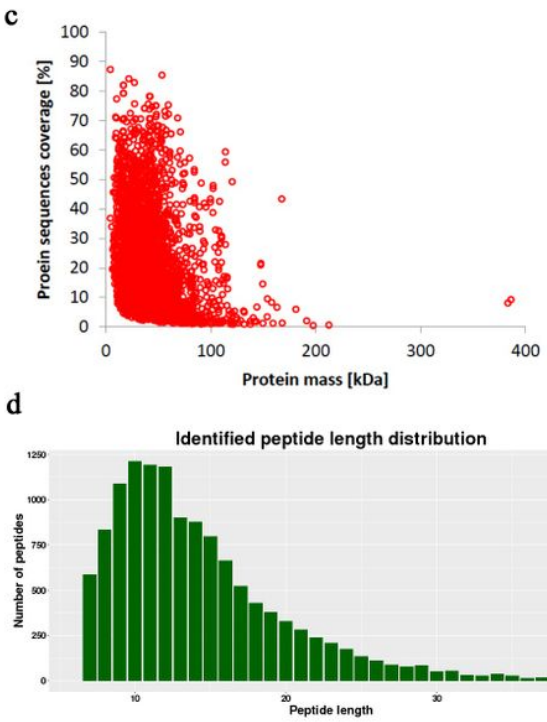


## Figure 1

Experimental strategy for quantitative proteome analysis and quality control validation of MS data. a Proteins were extracted from three biological replicates for each sample group. All protein samples were digested with trypsin and analyzed by LC/MS. b Pearson's correlations. c mass delta of all identified peptides. d length 511 distribution of all identified peptides.

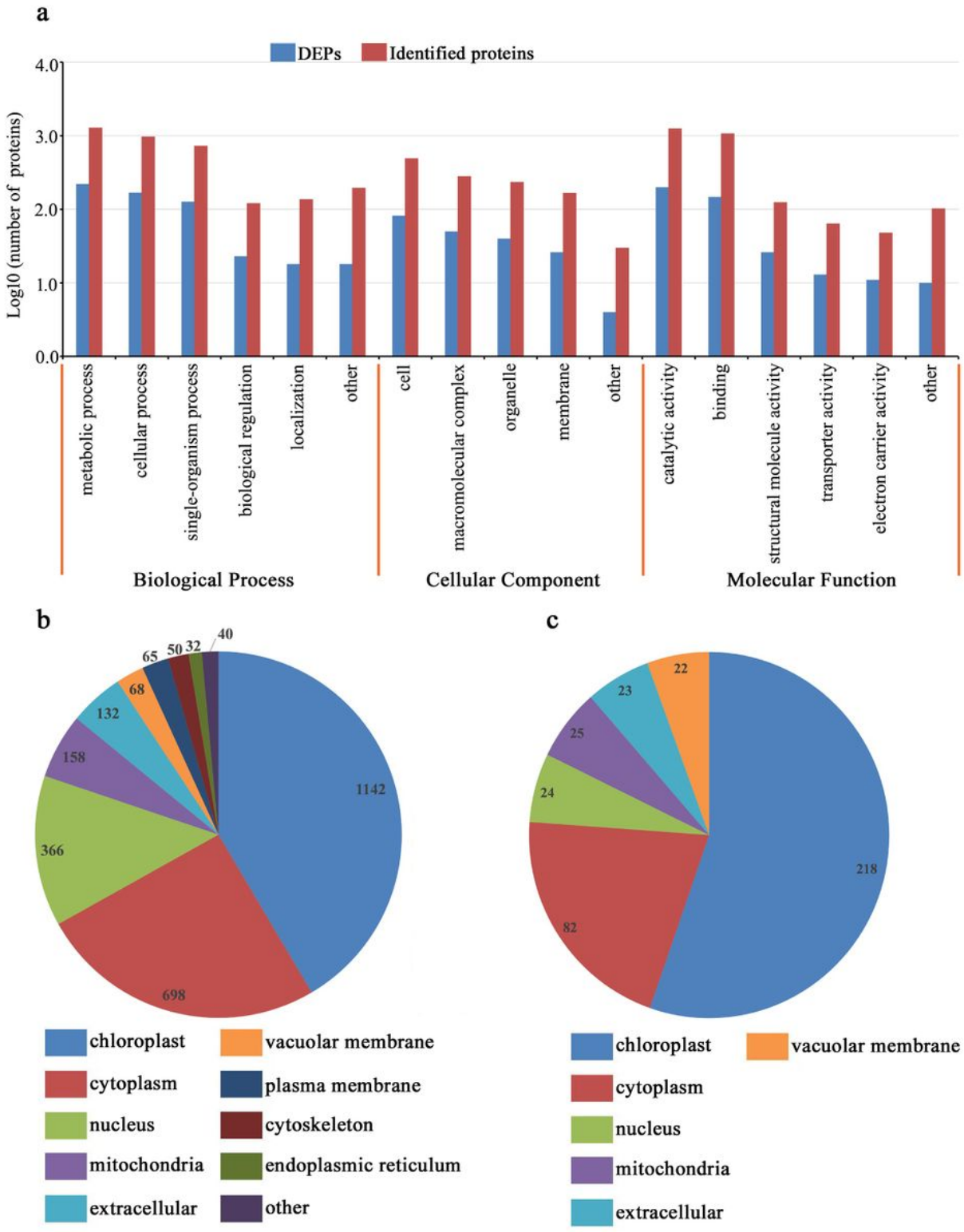


## Figure 2

Classifications of identified proteins and DEPs. a GO analysis of all identified proteins and DEPs. b Subcellular locations analysis of all identified proteins. c Subcellular locations analysis of all DEPs.

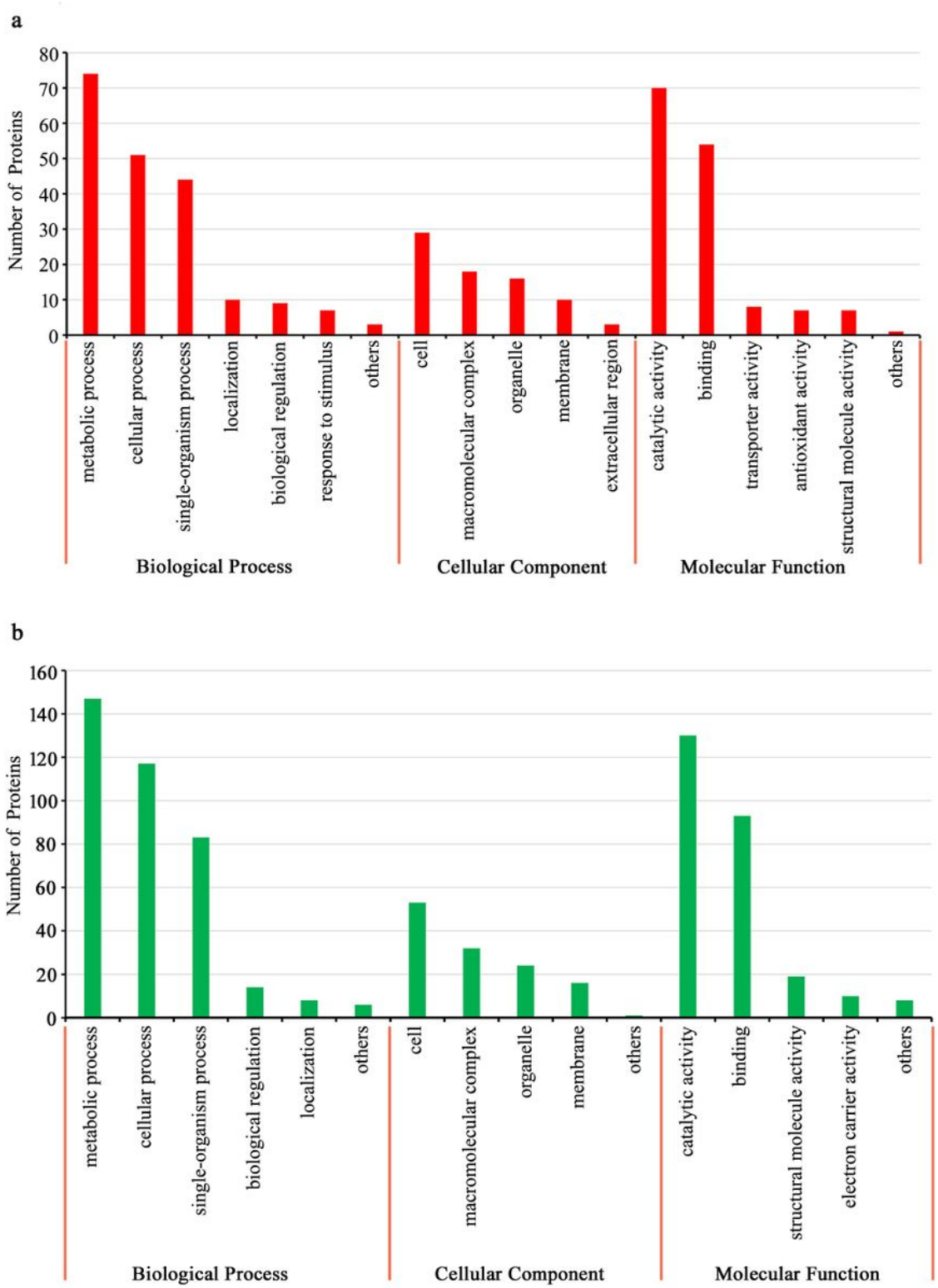


## Figure 3

GO analysis of up-regulated and down-regulated DEPs. a GO analysis of up-regulated DEPs. b GO analysis of down-regulated DEPs.

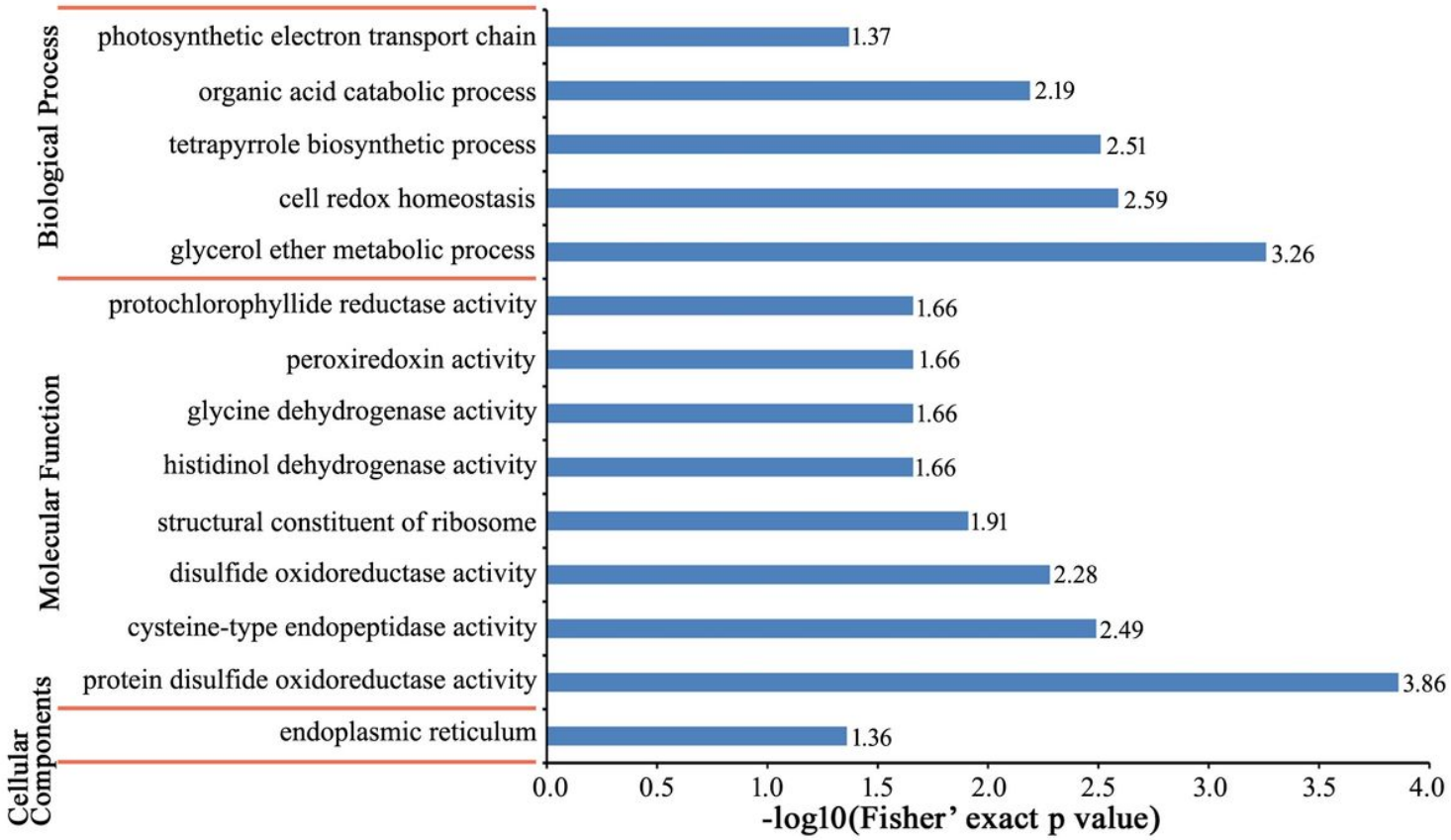


## Figure 4

GO enrichment analysis of DEPs. Significantly enriched GO terms of all DEPs.

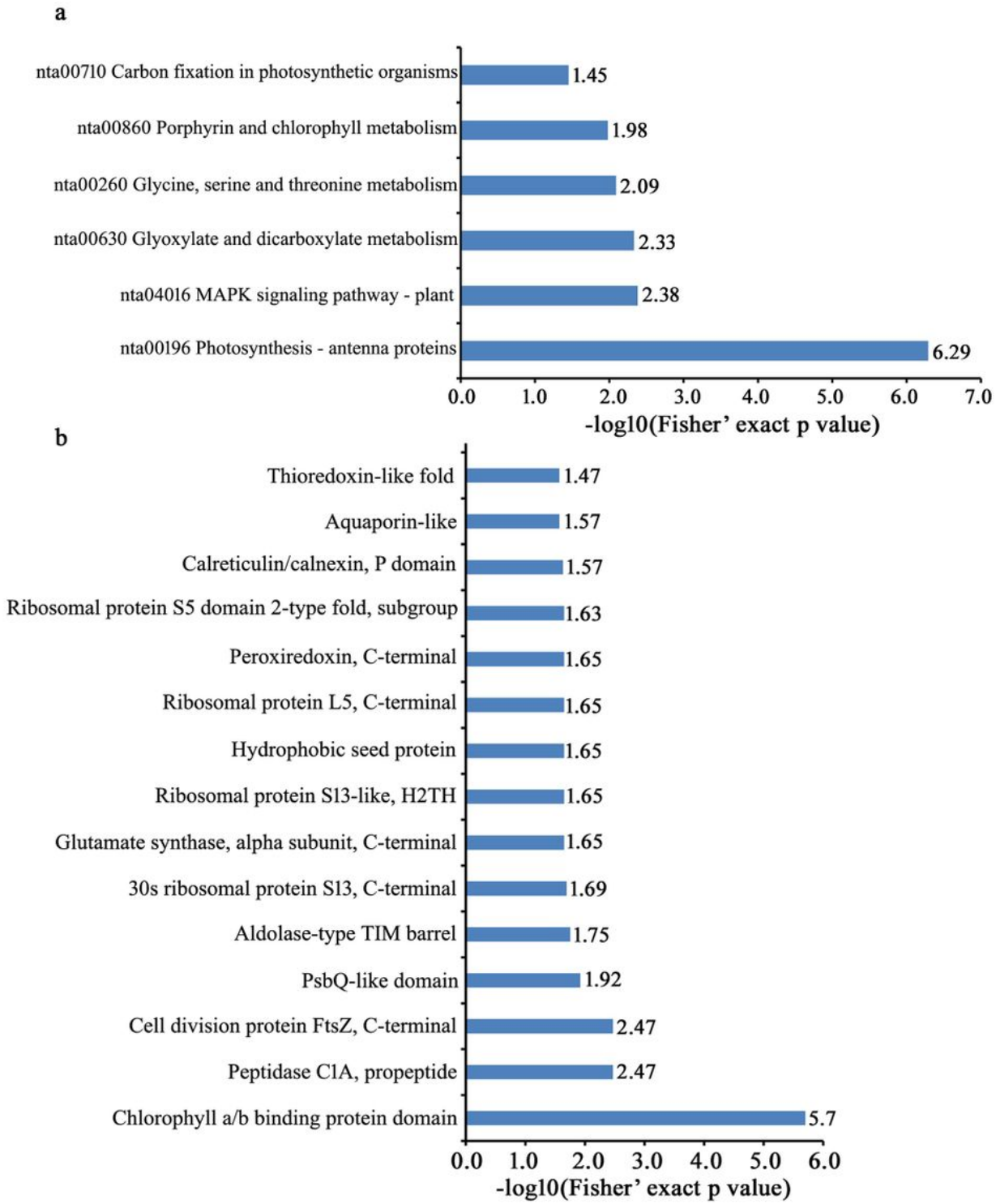


## Figure 5

Enrichment analysis of DEPs. a Significantly enriched KEGG terms of all DEPs. b Significantly enriched protein domain terms of all DEPs.

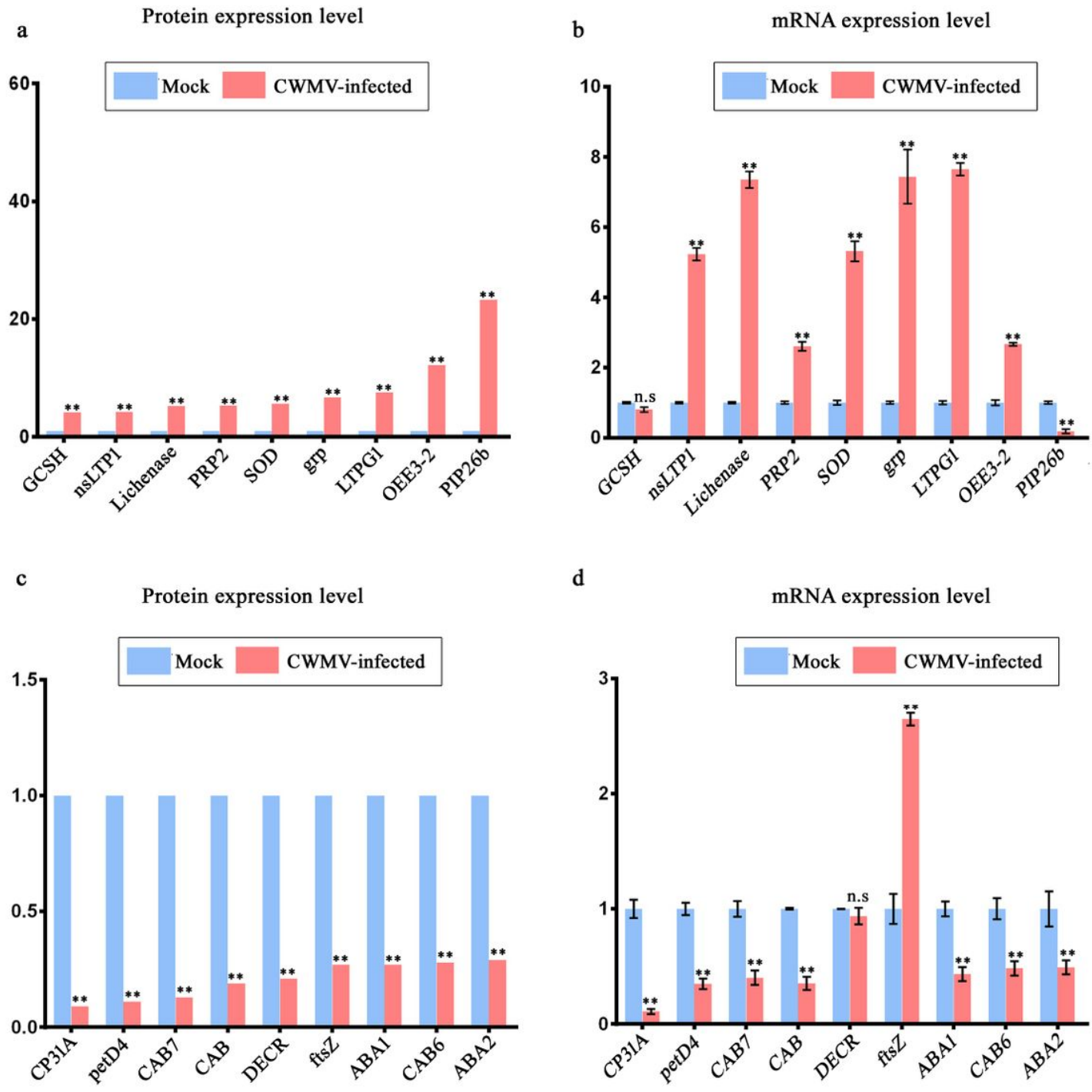


## Figure 6

Validation of N. benthamiana selected genes expression. a Nine up-regulated DEPs selected. b qRT-PCR showing genes encoding nine up-regulated DEPs selected. Each mean ± SD was from three biological replicates and each replicate had three technical replicates. **, p< 0.01; ns, not significant determined by the Student's t-test. c Nine down-regulated DAPs selected. d qRT-PCR showing genes encoding nine down-regulated DAPs selected. Each mean ± SD was from three biological replicates and each replicate had three technical replicates. **, p< 0.01; ns, not significant determined by the Student's t-test.

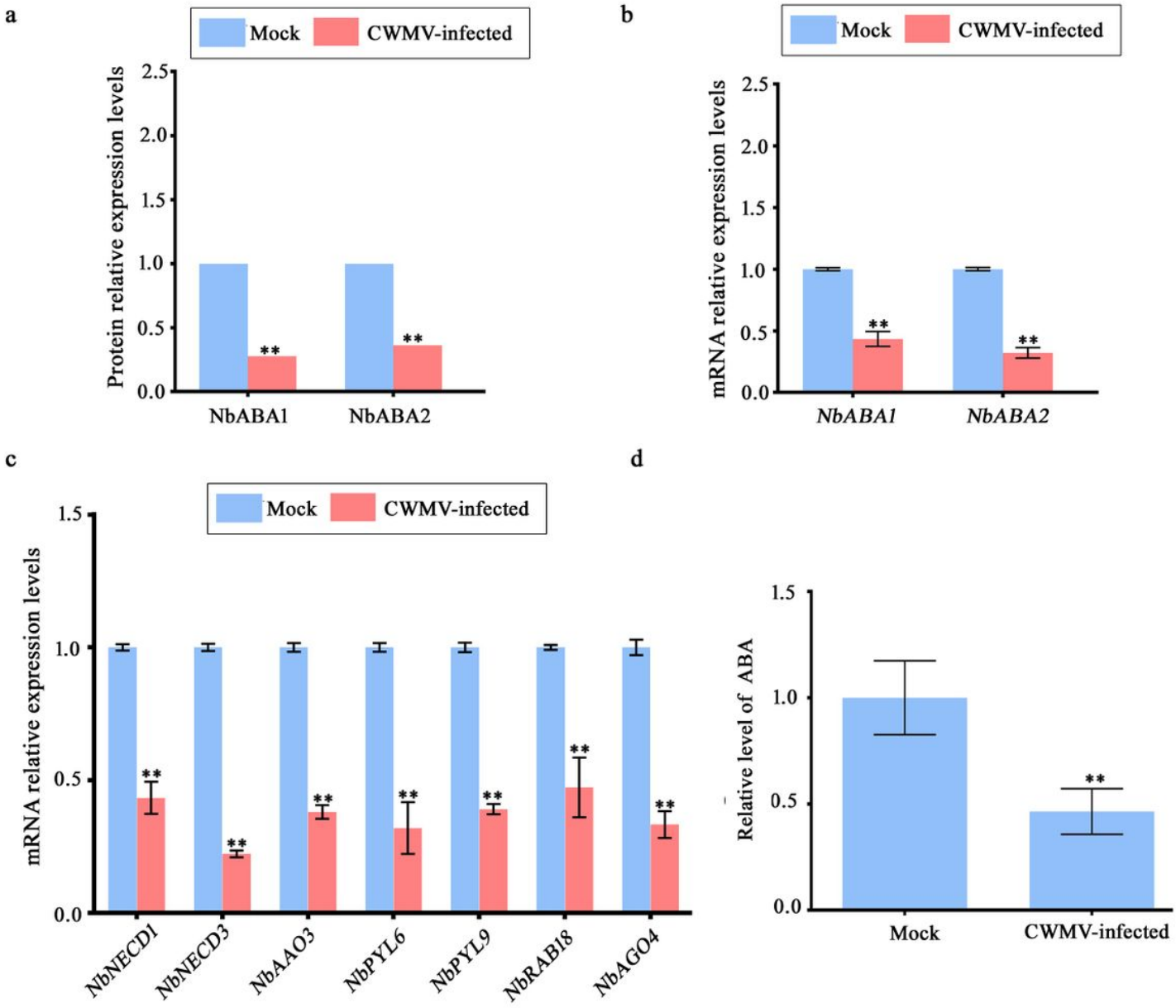


## Figure 7

Effects of CWMV infection on the ABA pathway. a Proteins (ABA1and ABA2) involved in the ABA signaling pathway that significantly changed responsive to CWMV infection. b qRT-PCR data showing the expression of NbABA1 and NbABA2 under CWMV infection. c qRT-PCR data showing the expression of ABA-pathway genes under CWMV infection. Each mean ± SD was from three biological replicates, and each replicate had three technical replicates. **, $p< 0.01$ determined by the Student's t-test. d detection of endogenous ABA production in mock and CWMV-infected plants. Each mean ± SD was from three biological replicates, and each replicate had three technical replicates. **, $p< 0.01$ determined by the Student's t-test.

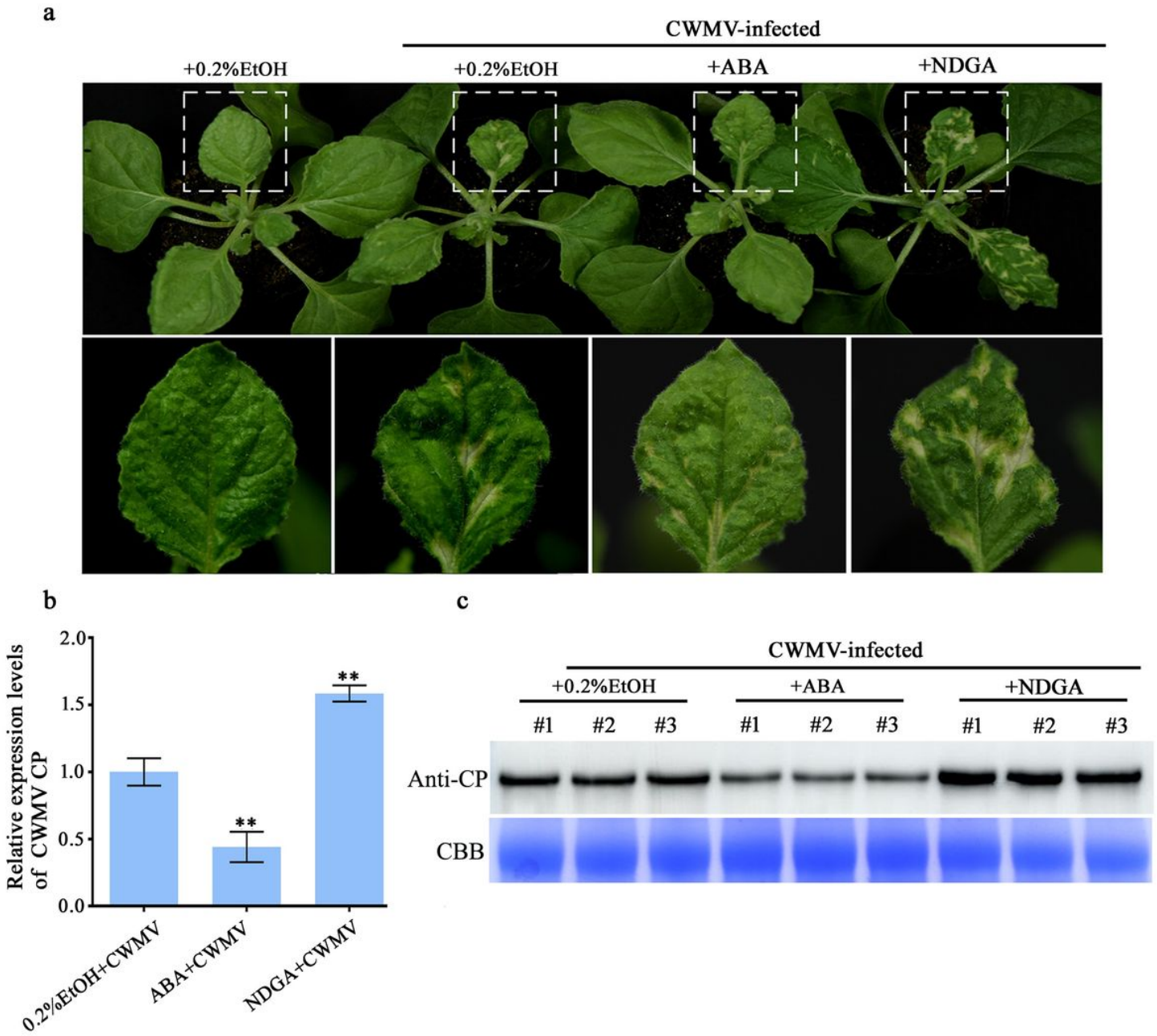


## Figure 8

Effects of ABA and its inhibitor application on CWMV infection in N. benthamiana. a Phenotype of N. benthamiana treated with 100 μM ABA or 10 mM NDGA or 0.2% EtOH (mock) followed CWMV inoculation at 21 dpi. b qRT-PCR results showing the mRNA expression of CWMV CP in pre-treated plants. Each mean ± SD was from three biological replicates, and each replicate had three technical replicates. **, $p < 0.01$ determined by the Student's t-test. c Western blot analyses of CWMV CP protein accumulation in the ABA or NDGA pre-treated CMWV-inoculated plants. CBB-stained loadings are shown at the bottom of the figure.

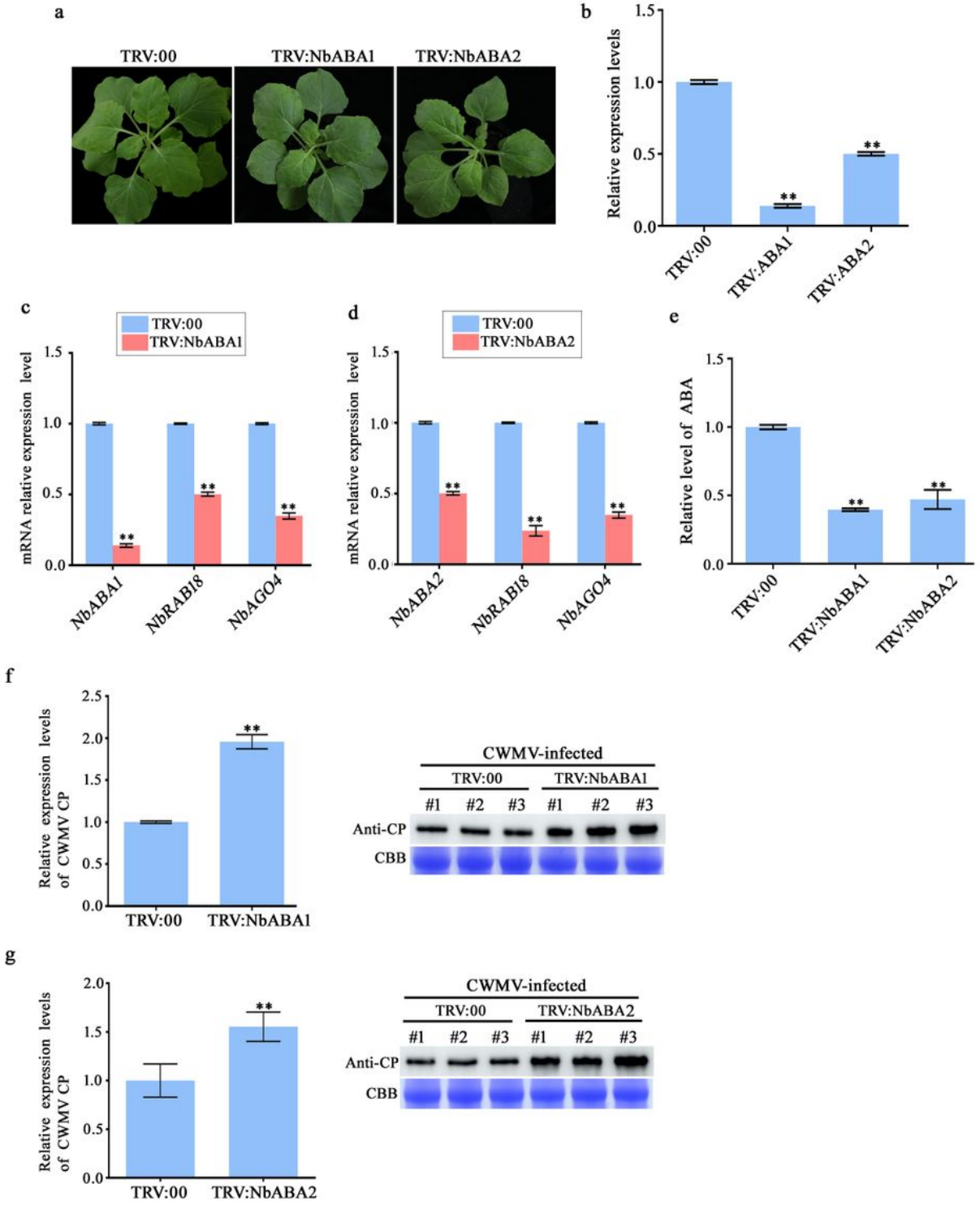


## Figure 9

Effects of silencing NbABA1 or NbABA2 on CWMV CP accumulation. a Phenotypes of NbABA1-silenced and NbABA2-silenced plant. Photograph taken at 7 dpai. b qRT-PCR showing mRNA expression of NbABA1 and NbABA2. Each mean ± SD is from three biological replicates, and each replicate had three technical replicates. **, $p<0.01$ determined by the Student's t-test. c qRT-PCR showing mRNA expression of NbRAB18 and NbAGO4 in NbABA1-silenced plants. d qRT-PCR showing mRNA expression of NbRAB18

and NbAGO4 in NbABA2-silenced plants. Each mean ± SD was from three biological replicates and each replicate had three technical replicates. **, p< 0.01 determined by the Student's t-test. e detection of endogenous ABA production in Control and NbABA1-silenced or NbABA2-silenced plants. Three independent biological replicates were analyzed for each treatment. **, p< 0.01 determined by the Student's t-test. f qRT-PCR showing mRNA (left) and western blot assay showing protein (right) expression of CWMV CP respectively in NbABA1-slienced plants. g qRT-PCR showing mRNA (left) and western blot assay showing protein (right) expression of CWMV CP respectively in NbABA2-slienced plants. Each mean ± SD is from three biological replicates and each replicate had three technical replicates. **, p< 0.01 and was determined by the Student's t-test. CBB-stained loadings are shown in the bottom of the figure.

## Supplementary Files

This is a list of supplementary files associated with this preprint. Click to download.

- Additionalfile5FigureS2.tif
- Additionalfile7FigureS3.tif
- Additionalfile3TableS2.xlsx
- Additionalfile6TableS4.xlsx
- Additionalfile4TableS3.xlsx
- Additionalfile10TableS5.xlsx
- Additionalfile11originalimages.docx
- Additionalfile1FigureS1.tif
- Additionalfile2TableS1.xlsx
- Additionalfile8FigureS4.tif
- Additionalfile9FigureS5.tif